A DIGITAL COMPUTER SIMULATION AND STUDY OF A DIRECT-ENERGY-TRANSFER POWER-CONDITIONING SYSTEM

William W. Burns, III Harry A. Owen, Jr. Thomas G. Wilson

Department of Electrical Engineering
Duke University, Durham, N. C.

G. Ernest Rodriguez John Paulkovich

Spacecraft Technology Division
Goddard Space Flight Center, NASA, Greenbelt, Md.

ABSTRACT

Because of the many complex subsystem interactions which occur within modern electronic power-processing systems, it is often quite difficult to accurately predict total system performance. A digital computer simulation technique, which can be used to study such composite power-conditioning systems, is applied to a spacecraft direct-energy-transfer power-processing system. The results obtained duplicate actual system performance with considerable accuracy. The validity of the approach and its usefulness in studying various aspects of system performance such as steady-state characteristics and transient responses to severely varying operating conditions are demonstrated experimentally.

INTRODUCTION

During the past two decades, the field of power electronics has been evolving and expanding into an increasingly more important element of modern electro-technology. New and more powerful methods of analysis and design have been developed, resulting in improved power-conditioning equipment which often finds new and diverse applications in many areas of electronics. Recently, for reasons of economic efficiency and system reliability, there has been considerable interest in developing standardized power-conditioning circuits and systems for space applications. These standardized designs would obviate the need for costly, but often still not optimum, custom designs for every new power system required [1]. Some standardized power-conditioning modules have already been developed which satisfy a wide range of mission requirements, thus eliminating much of this cost and at the same time making available to the system designer a pool of fully tested equipment with proven reliability [2,3].

In trying to meet specific mission requirements with such standardized modules, it becomes increasingly more important to be able to study the performance of power systems as a whole, rather than the various subsystems individually. Because of the many subsystem interactions within such composite systems, it is often quite difficult to predict the total system response even though the behavior of the individual subcircuits may be familiar and well documented. However, the behavior of the power-conditioning system as a whole when in steady-state operation or when subjected to transient disturbances such as step changes in load or variations in the primary and secondary source characteristics must be fully investigated before the integrity of the aggregate power-conditioning system can be ensured. It is the purpose of this paper to present one approach to this problem of studying aggregate power-conditioning systems, and to demonstrate the validity and usefulness of this approach.

In considering the size and complexity of modern power-conditioning systems, the digital computer quickly comes to mind as an attractive and viable tool for such a study. Even though much progress has been made recently in developing and applying powerful analytical tools to the study of particular converter and inverter circuits [4,5], none of these techniques is applicable to a general composite power-conditioning system which can be described by an n^{th}-order system of nonlinear differential equations. On the other hand, the rapid development of digital computer circuit and system analysis programs over the past few years has given the electronics engineer the ability to examine more precisely very large analysis problems which had previously been intractable or too costly to pursue. Particular computer studies, both digital and analog, have also been presented recently which enhance the understanding of and aid in the design of individual power converter circuits [6,7,8], but again there have been no published results concerning simulations and studies of entire power-conditioning systems. This paper describes in considerable detail the application of a general "digital analog simulator" program, derived from IBM's Continuous System Modeling Program (CSMP) [9], to the study of an aggregate power-conditioning system being developed at the NASA Goddard Space Flight Center for use on the International Ultraviolet Explorer (IUE) Spacecraft.

This work was supported in part by the National Aeronautics and Space Administration under Research Grant NGL-34-001-001 to Duke University.

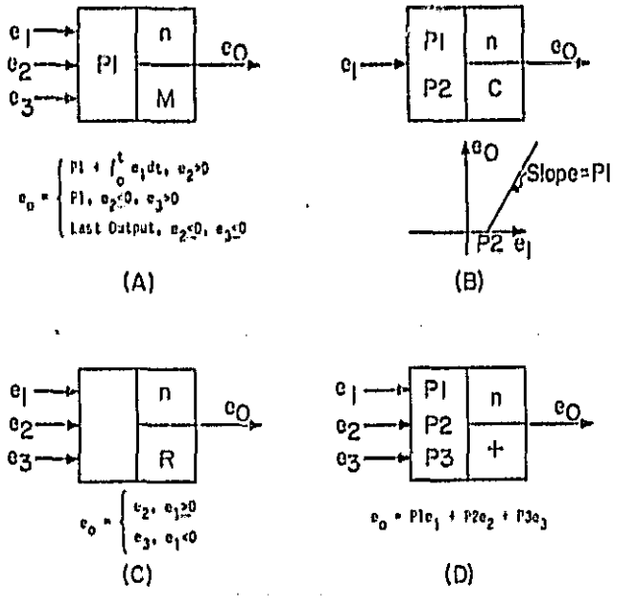

Fig. 1. Examples of the types of functional "blocks" available for implementing system descriptions in the computer program format. (A) Type M, mode-controlled integrator. (B) Type C, clipper. (C) Type R, relay. (D) Type +, weighted summer.

THE SIMULATION TOOL

As mentioned above, the tool used in this work is an interactive digital computer program based on an IBM application program, CSMP, as developed for use on the IBM 1130 system. The computer studies presented in this paper were run on a Digital Equipment Corporation PDP-11/45 digital computer equipped with a Tektronix 4013 storage-tube graphics console using a substantially modified version of the 1130 CSMP. With appropriate modifications to the input data, however, similar studies could be conducted on a number of other computing machines including the IBM 360/370 systems.

The structure of this program is such that the particular dynamic system being investigated is entered into the computer in terms of the system state equations. These equations are implemented by means of an appropriate connection of input/output functional relationships, much as is done when using an analog computer. Thirty types of functional "blocks" are available for this purpose, four of which are illustrated in Fig. 1. These symbolic blocks display all of the information required to completely program a system simulation. Each block is given a single-character type designation, e.g. M, C, R or +, as shown in Fig. 1, which is uniquely defined within the program and corresponds to a particular function. Each block also must be assigned an individual identification number n. The numbering of the blocks need not be sequential since the program uses a sorting algorithm to determine the proper order for evaluating the

$$\frac{d^2x}{dt^2} - \epsilon(1-x^2)\frac{dx}{dt} + x = 0$$

(A)

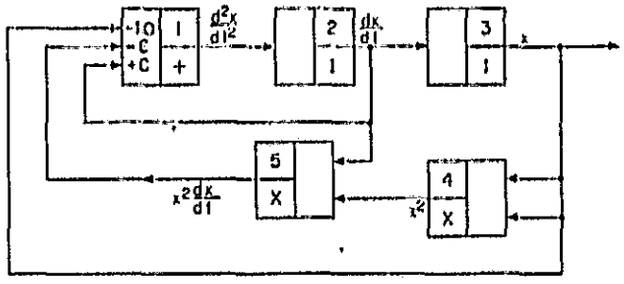


```
                    CONFIGURATION SPECIFICATION

BLOCK      TYPE     INPUT 1    INPUT 2    INPUT 3
  1          4          3          5          2
  2          1          1          F          0
  3          1          2          0          0
  4          X          3          3          E
  5          X          2          4          E

                    INITIAL CONDITIONS AND PARAMETERS

BLOCK      IC/PAR1          PAR2             PAR3
  1     -0,1000000E 01   -0,5000000E 01    0,5000000E 01
  3      0,1000000E 01    0,0000000E 00    0,0000000E 00

(    0,1000000E-01 )INTEGRATION INTERVAL
(    0,3000000E 02 )TOTAL TIME
(    0,1000000E-01 )PRINT INTERVAL

Y-AXIS VARIABLE(S) PLOTTED
BLOCK NO,(VERT,)     MIN,VALUE          MAX,VALLE
  2                  -0,1000000E 02     0,1000000E 02
BLOCK NO,(HORZ,)     MIN,VALUE          MAX,VALLE
  3                  -0,1000000E 02     0,1000000E 02
```

(C)

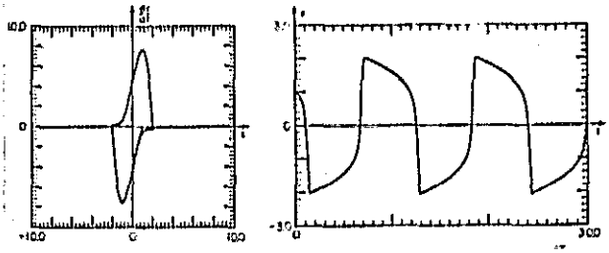

Fig. 2. Example of the application of the simulation tool to a second-order nonlinear system. (A) Van der Pol's equation. (B) Block diagram for solution of equation. (C) Program input statements for output shown in (D). (D) Output data in form of X-Y plot. (E) Output data in form of Y vs time plot.

output of each block. Specifying the input connections to each block of the system representation and the associated parameter values completes the simulation diagram. Depending on the block type, from zero to three inputs and from zero to three parameters must be specified. The

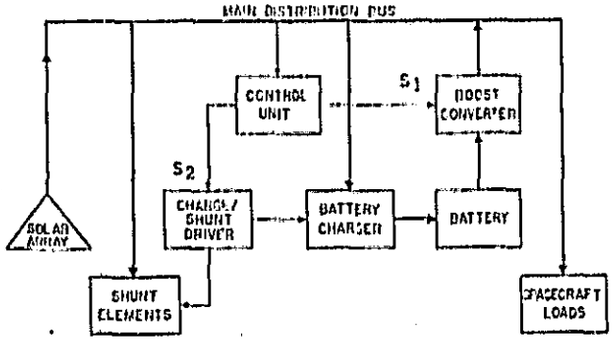

Fig. 3. Block diagram representation of the DET system under investigation with bold lines indicating power channels.

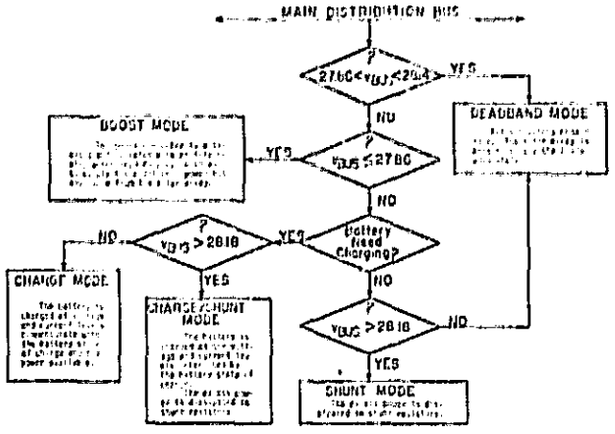

Fig. 4. Decision flow chart illustrating the operational modes possible within the DET system, and the conditions which activate them.

connections to the inputs, shown symbolically in Fig. 1 by input variables e_1, e_2 and e_3, correspond to outputs from numbered blocks within the simulation diagram. The parameters, symbolized by P1, P2 and P3, correspond to real constant numbers which are a part of the function represented by the block.

To clarify this procedure, a simple example of a system represented by a second-order nonlinear differential equation is shown in Fig. 2. In this example, blocks 2 and 3 are standard integrators, designated type I, which integrate the input signal continuously from the initial time to the final time. The initial condition for each integrator can be specified as parameter P1 of the respective blocks. In this example, the initial conditions have been specified as 0.0 and 1.0 for blocks 2 and 3,respectively,as shown in Fig. 2(C). Blocks 4 and 5 are multipliers, designated type X, which simply multiply one input by the other. The parameters P1, P2 and P3 associated with block 1, are given values of -1.0, $-\varepsilon$ and ε respectively, where ε is a numerical constant of the system. For the case shown in Fig. 2(C), ε has been given a value of 5. All of the input data described above are entered into the computer in fixed format which greatly facilitates this routine task.

After selecting an appropriate integration interval and a final solution time, the computer begins integrating the programmed system state equations using a second order Runge-Kutta integration scheme. The numerical value of the output of each of the blocks comprising the system representation is available as a tabulated printout and/or a graphical display at each integration interval. The speed with which the computer can perform these integrations is a function of the system complexity and the size of the integration step specified. Systems with short time constants may require relatively small integration steps in order to accurately compute fast transients, and therefore would be subject to relatively long run times if the desired system response extends for a long period of time. Some experimentation with the integration interval is usually required to achieve a satisfactory combination of accuracy and computational speed.

Two of the most attractive features of this program are its interactive capabilities as originally designed for the IBM 1130, and the flexibility provided in the choice of the output display formats as designed for the PDP-11/45 computer and Tektronix 4013 graphics unit. The interactive nature of the program enables the user to interrupt a simulation run at any time to modify the system description and thus perform on-line experimentation. Sixteen switches on the computer control panel are used for this purpose whereby such items as system parameters, initial conditions, and run controls can be adjusted. Additionally, the user may choose to display the output data of a given run in the form of an X-Y plot, with as many as five system variables plotted versus any other system variable with time an implicit parameter; or he may choose to display as many as five of the system variables as functions of time. In either case, numerical printouts of the same five or five different output variables are also available. Two sample output displays for the example of Fig. 2 are presented in Fig. 2(D) and (E).

THE SYSTEM UNDER INVESTIGATION

The system being simulated with this program is the main bus regulator for the International Ultraviolet Explorer Spacecraft which is a joint mission between the Goddard Space Flight Center (GSFC/NASA), the British Science Research Council, and the European Space Research Organization. This system is a direct energy transfer (DET) system whereby the primary source of electrical energy, a solar array in this case, is coupled through a main distribution bus directly to the spacecraft electrical loads. The various power-conditioning subsystems, shown in Fig. 3, are activated only as needed, thus requiring the system to process only that amount of power which is needed to maintain the power bus at the specified voltage level. The flow chart in Fig. 4 indicates the various modes of operation which are possible within this system.

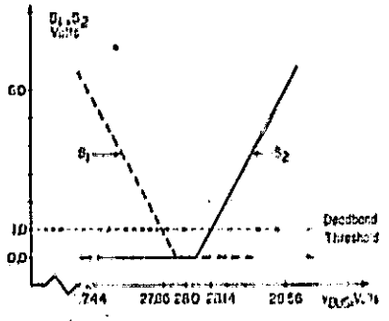

Fig. 5. Control unit outputs S1, to boost converter, and S2, to charge/shunt driver, as a function of bus voltage.

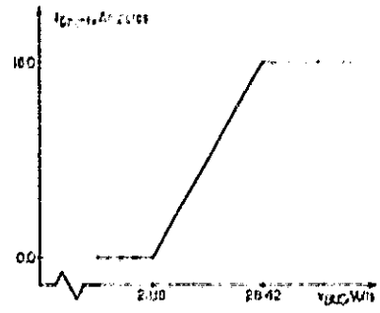

Fig. 6. Dissipative shunt regulator current as a function of bus voltage.

The specified main bus voltage range for this mission is 28±0.56 volts. The power system control unit continuously monitors this voltage level and generates appropriate signals to activate one of five different modes of operation designed to meet this regulation requirement under widely varying operating conditions. This control unit function is depicted graphically in Fig. 5. For a voltage of 28±0.14 volts, the system is said to be in the *deadband mode* whereby all of the electrical energy required by the spacecraft loads is available from the solar array with no additional energy from the array to be dissipated and no supplementary energy from the secondary source required. Under these conditions, signals S_1 and S_2 from the control unit lie below the one-volt deadband threshold level, as shown in Fig. 5, and all of the subsystems remain idle. If, however, the solar array is unable to adequately supply the loads, the bus voltage falls and the control unit generates signal S_1 which activates the *boost mode* of operation, and drives the boost converter with an adaptive duty-cycle control signal as determined by the secondary source voltage and the amount of additional power required. The secondary source of energy in this case is a pair of rechargeable nickle-cadmium storage batteries which have terminal voltages between 17 and 25 volts, depending on the state of charge. If, on the other hand, the solar array is generating energy at a faster rate than is required by the spacecraft and the bus voltage rises above 28.14 volts, the excess energy must be funneled off to prevent an over-voltage condition on the main bus. Under these conditions, the control unit, in conjunction with the charge/shunt driver and the battery charger subsystem, channels an appropriate amount of this energy into the secondary storage battery. Analog signals corresponding to the battery state of charge and the amount of excess power available from the solar array are combined to provide the duty-cycle control of the battery charger which ensures the proper charging rate. This mode of operation is referred to as the *charge mode*. If still more power is available than is required to properly charge the battery, the bus voltage continues to rise and additional energy must be dissipated, thus activating the *charge/shunt mode* of operation. When the bus voltage exceeds 28.18 volts, the shunt elements are activated and dissipate the excess power through resistors which are mounted on the spacecraft structure. The array of shunt elements is capable of dissipating up to a total of 450 watts of power as a linear function of the bus voltage as shown in Fig. 6. When the solar array is generating unneeded energy, but at the same time the battery is fully charged, the fifth mode of operation is activated. In this case, all of the unneeded energy is dissipated in the shunt resistors and the system is said to be in the *shunt mode*.

On examining the schematic diagram of this system as shown in Fig. 7, one quickly recognizes that classical circuit analysis techniques may not be satisfactory tools for studying the complex interactions of the various subsystems. Nevertheless, a careful examination of switching transients which may occur on the main bus as a result of severely varying operating conditions is a necessary part of verifying the compliance of the system to its performance specifications. Of particular concern in a system such as this is its response to uncontrollable external inputs such as the intensity of sunlight on the solar panels or the state of charge of the secondary storage battery. Thus, the technique described in this paper for simulating the entire power system as a whole and systematically computing transient responses and steady-state characteristics is a very profitable approach and enables the system engineer to more thoroughly investigate his system while it is still in the design stage.

SYSTEM MODEL AND MATHEMATICAL REPRESENTATION

The Model

In order to effectively study the physical system described above, it is necessary to develop an appropriate model which is simple enough to yield a tractable mathematical representation but at the same time detailed enough to enable an accurate description of those aspects of the system behavior which are of interest. It is clear that any given system can be modeled in many different ways depending on which system properties are considered more important or of most interest. Frequently, however, it is difficult to immediately determine the full significance of each component of the system, and therefore it often is necessary

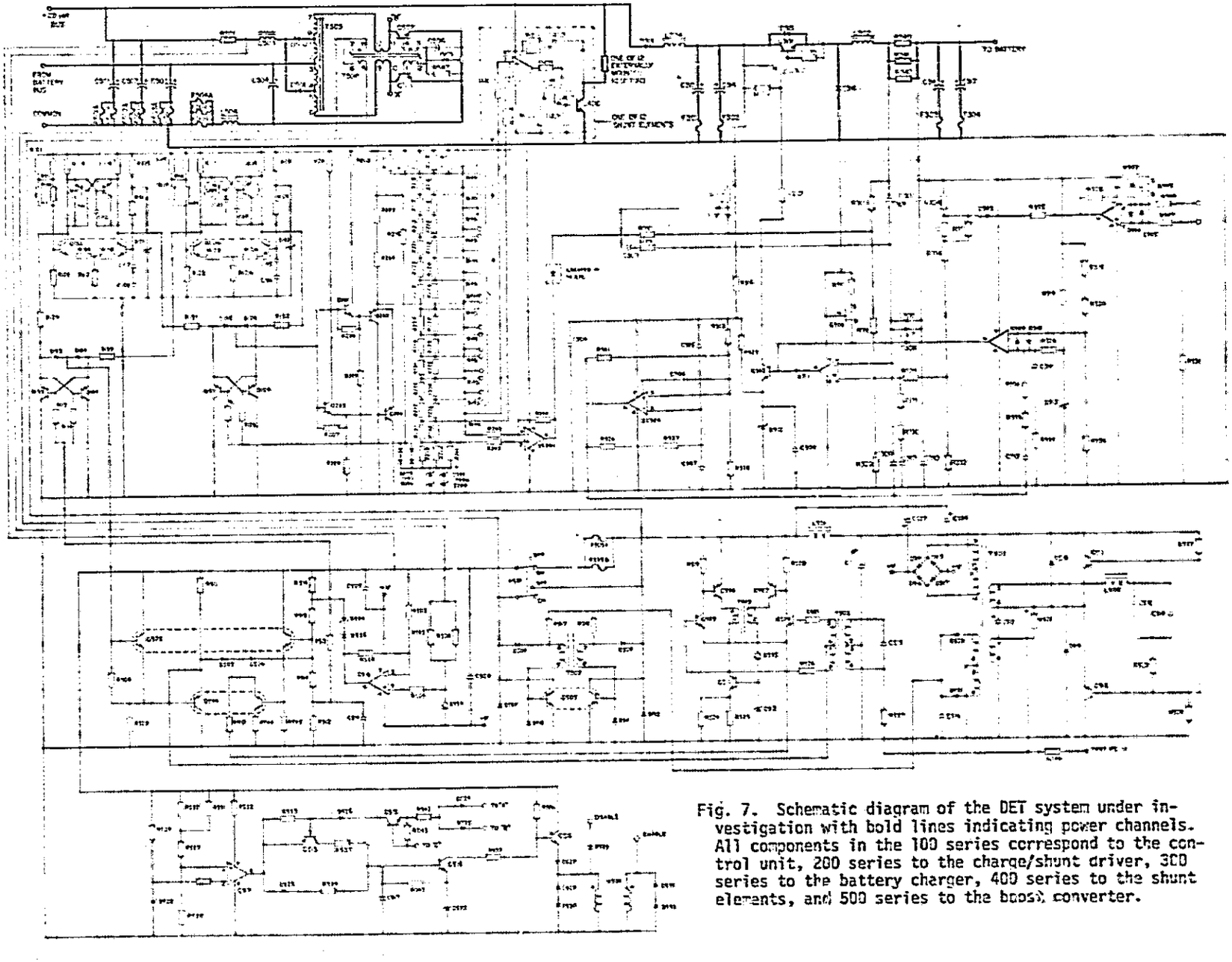

Fig. 7. Schematic diagram of the DET system under investigation with bold lines indicating power channels. All components in the 100 series correspond to the control unit, 200 series to the charge/shunt driver, 300 series to the battery charger, 400 series to the shunt elements, and 500 series to the boost converter.

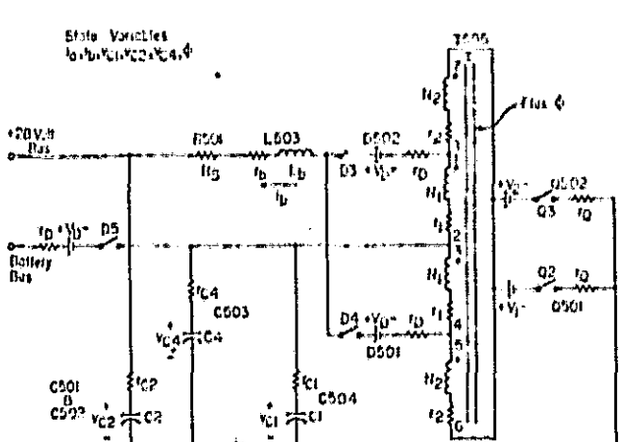

Fig. 8. Idealized model of the power-handling subnetwork of the boost converter subsystem. Actual component labels from Fig. 7 are shown next to the corresponding component model.

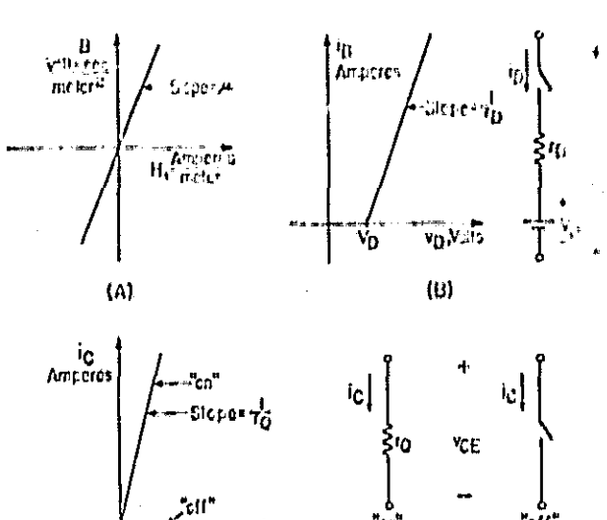

Fig. 9. Idealized models for (A) magnetic core of transformer T, (B) semiconductor diodes D3, D4, and D5, and (C) transistor Q2 and Q3 of Fig. 8.

to revise the system model at various stages of its development when new evidence indicates that incorrect assumptions have been made or that unnecessary details which unduly complicate the model have been included. By such a process, an appropriate model of the direct energy transfer system described in the preceding section was developed. The complete model consists of a tenth-order nonlinear network which approximates the power-handling subnetworks of the system, and several resistive input/output relationships which represent the system control functions.

As an example of the modeling approach taken in this work, consider the schematic diagram of the boost converter subsystem as shown in Fig. 7. All of the power-handling subnetworks of this system are drawn with bold lines at the top of the diagram. The boost converter subsystem consists of all of the components labeled with a 500-series number. The power subnetwork is shown in the upper left-hand portion of the diagram, while the control subsystem is shown in the lower third of the figure. The model developed for the power-handling portion of this subsystem is shown in Fig. 8. Each of the capacitors has been modeled as an ideal lumped capacitance in series with a small ideal lumped resistance which approximates the equivalent series resistance (ESR) of the actual component. Similarly, small winding resistances have been included in the models of the inductors and the transformer, but the winding capacitances have been neglected. The autotransformer has been modeled as a linear device defined by the flux density versus magnetic field strength characteristic shown in Fig. 9(A). The semiconductor diodes have been approximated with a static nonlinear resistive characteristic as defined in Fig. 9(B). Similarly, the transistors are considered to be either fully on or fully off for the purposes of this study, and each is modeled as an open circuit for the off condition and as a small saturation resistance for the on condition as illustrated in Fig. 9(C). It should be noted that if detailed information concerning the performance of the semiconductor devices in this system is desired, the model of each semiconductor component can be changed to include those properties of the device which are of particular interest. The work described in this paper, however, is concerned primarily with the transient behavior of the main bus voltage, and the dynamic performance of the semiconductor components has not been considered. The voltage sources V_1 and V_2 shown in Fig. 8 represent the voltages induced across control windings 9-10 and 12-11 respectively on transformer T504 which is shown at the top of Fig. 7. These induced voltages are assumed to be constant during the on-time of the appropriate transistor and are therefore modeled as constant voltage sources. Resistor R_5 is a small current sensing resistor which provides a current limiting signal to the control unit of this subsystem.

The control unit for the boost converter subsystem is modeled as a purely resistive network. The purpose of this subnetwork is to provide the duty-cycle control of the two power transistors shown in Fig. 8. This is accomplished by generating a constant-frequency triangular waveform with a fixed peak-to-peak amplitude and adding to it a threshold level, V_d, which is a function of the bus voltage as shown graphically in Fig. 10. As the bus voltage falls, the threshold level falls, allowing the power transistors to turn on for a greater portion of each cycle of the triangular waveform. This increased duty cycle enables the converter output current to increase to a new level which satisfies the increased load requirement.

As can be seen in Fig. 7, the various control circuits of the complete power system are often quite complex, and the transfer func-

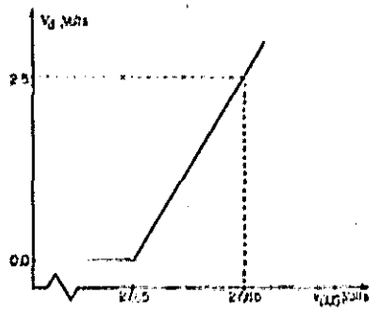

Fig. 10. Threshold level V_d of the boost converter controller as a function of bus voltage.

tions derived are by no means immediately obvious. In most cases a substudy was conducted to reveal the salient features of these control subcircuits and to precisely determine the appropriate transfer characteristic. Some of these studies involved experimental measurements, while in other cases digital computer circuit analyses were run to reveal the significant circuit relationships. In all cases, however, the assumption that these circuits are essentially purely resistive was carefully verified.

In a similar manner, models have been developed for the battery charger subsystem, the shunt elements, the charge/shunt driver, and the main control unit. The complete system model includes controllers to determine the duty-cycle of the power transistors in the boost converter and the battery charger subsystems, and a controller to determine the value of the shunt dump resistance at all times.

The Mathematical Representation

To analyze the model presented in the preceding subsection, it is necessary to construct a mathematical representation for it. As described above, the control subcircuits of this system have been modeled as purely resistive networks. Thus, the behavior of these subnetworks is completely specified by a set of nonlinear functional equations which may be derived from the laws of the elements in these circuits and the laws of interconnection of them; or they may be approximated from experimentally measured transfer characteristics of the circuits. Given these equations, all of the voltages and currents in the control subnetworks can be computed under all possible operating conditions. But in practice, only those combinations of currents and voltages which explicitly determine the control signals of interest have been represented mathematically. The coefficients of these functional equations are determined from appropriate combinations of the actual circuit component values, including variable elements such as the battery state of charge, bus voltage, and solar array output current. Thus, the currents and voltages of interest in these circuits, and therefore the system control signals, change value as pertinent system variables change; and these changes in control signals give rise to the various modes of operation of the system as described in the third section of this paper.

To complete the mathematical representation of the model, the power-handling subnetworks must be considered. Since the combined subsystems have been modeled as a tenth-order nonlinear dynamic network, a set of ten independent nonlinear differential equations is required to mathematically specify the behavior of the network. Having developed these state equations from the laws of the elements and the laws of interconnection of the network, and given the values of the state variables at some initial time t_0, the currents and voltages throughout this network can be determined for any time $t > t_0$. But because of the many different operating conditions possible within this system, one set of state equations is not sufficient to completely characterize the system at all times. These different modes of operation are the result of a transistor or a diode switching on or off, and thus effectively changing the topology of the power-handling subnetworks and consequently the laws of interconnection of them. Therefore, a set of state equations must be written for each possible mode of operation within the system, and the state variables must be continuous through a transition from one mode to another as dictated by the control functions; i.e., the final value of state $\underline{x}$ for one mode of operation must be the initial state $\underline{x}_0$ for the next mode. With these sets of differential equations and the set of functional equations described above, the entire system model is accurately represented mathematically at all times and for all operating conditions. The next section describes how this comprehensive mathematical representation is implemented in the digital computer.

PROGRAMMING THE SYSTEM

As discussed earlier in the paper, the program used in this work may be considered to be a digital analog simulator in that the system solution is computed on a digital computer, but at the same time the program input format resembles analog computer connection diagrams. Thus, given the mathematical representation of the system as presented above, an analog-type connection diagram can be drawn as an intermediate step to programming the system. An example of this procedure for one of the system state equations is shown in Fig. 11. In Fig. 11(A) are the differential equations which determine the trajectory of the state variable v_{C1} of the boost converter power subsystem through all possible modes of operation of that subsystem. The connection diagram in Fig. 11(B) illustrates the way in which each of these differential equations is constructed from the pertinent system state variables and their associated coefficients which are determined numerically from appropriate combinations of the circuit component values. For example, the derivative of the voltage across capacitor C1 during the time transistor Q2 of Fig. 8 is on is a weighted sum of the currents through the inductors L_a and L_b, and the flux in transformer T. Block n_1 of Fig. 11(B) performs this summation where

$$P1 = \frac{1}{CT}$$

$$P2 = -\frac{N_1}{(N_1 + N_2)CT}$$

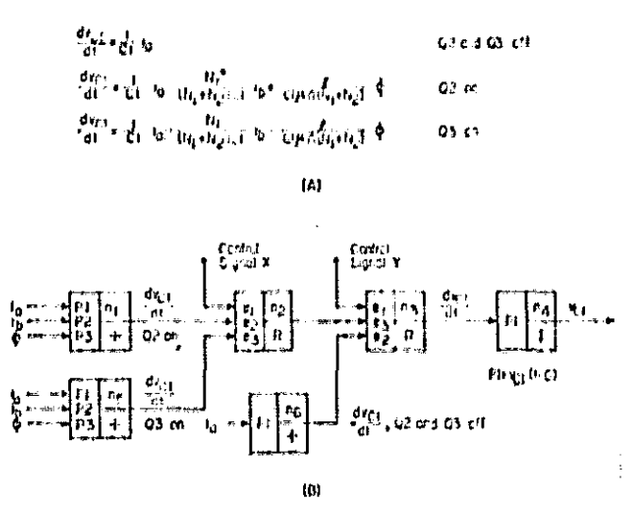

(A)

(B)

Fig. 11. Diagramming the state equations. (A) Differential equations describing the trajectory of state variable v_{C1} of Fig. 8 for three different operating conditions. (B) Block diagram representation of these equations.

and $$P3 = \frac{\ell}{C_1 \mu A (N_1 + N_2)}$$

The parameters ℓ, μ, and A represent, respectively, the mean magnetic path length, the permeability, and the cross-sectional area of the magnetic core of transformer T. Similarly, blocks n_5 and n_6 compute the derivative of this state variable for other operating conditions. Functional relay blocks are used to select the proper combination of variables at each instant of time as determined by the appropriate control function, thus simulating the switching semiconductor components of the system. In this case, control signal Y determines if either transistor Q2 or Q3 is on ; and if so, control signal X determines which one. These decisions are made at each computational time increment, and thus the correct value of the derivative of v_{C1} with respect to time is available for all time and all operating conditions. The output of relay block n_3 is integrated numerically to yield the continuous trajectory of the state variable v_{C1}. Continuity from one mode of operation to another is maintained through the memory of the integrator; i.e., the last output of the integrator for one operating condition becomes the initial condition for the next mode. In a similar manner, the functional representations of the control subsystems which generate the signals X and Y are diagrammed and connected to the appropriate relay blocks in the state equation diagrams.

When the entire system is diagrammed in this manner, it is then a simple matter to complete the programming procedure. After labeling each of the blocks in the connection diagram, the entire system description can be entered into the computer through preformatted statements as illustrated in Fig. 2(C). When the last block description is entered, the interactive program asks the user to enter the integration interval, the final solution time, and the output data options and format. After processing these entries, the computer begins calculating the system state trajectory and displaying the output data requested. The user can observe this data as it is being computed and has the option of interrupting the run at any time to modify the system description or output requests as suits his needs. In this way, on-line experimentation can be conducted as is described in the following sections.

EXPERIMENTAL VERIFICATION

To verify the ability of the computer representation described above to simulate actual system performance, a series of system tests were conducted on the assembled DET prototype unit and duplicated on the computer model. A comparison of the measured and computed results from two of these tests is presented in this section. The tests were designed to activate each of the system modes of operation, and thereby enable an examination and evaluation of all phases of the computer model. The data recorded during these tests are displayed in Figs. 12 through 17. The (A) portion of each figure is an oscillogram of the experimentally measured response of the actual DET power-conditioning system, while the (B) portion of each figure is the corresponding graphical computer output for the simulated system response. The computer generated output has been photographically reproduced to yield a grid of the same width as the experimental oscillograms. This means that the horizontal time axis in parts (A) and (B) of the same figure are identical. In each of these oscillograms and computer displays, the same four system variables--load current, shunt current, battery current and bus voltage--are plotted versus time with the same vertical scale factors of volts or amperes per division. These variables and their associated scaling are presented in Table I for easy reference when examining the data displays. It should be noted that the computer generated grid does not have the same vertical to horizontal ratio as the oscilloscope grid; i.e., the actual spacing between major vertical divisions in part (B) of each figure is greater than that in part (A). Thus, the various computer generated plots appear elongated in the vertical direction. The third waveform in each of the displays is the secondary-battery current which has been designated as positive when charging and negative when discharging the battery.

The first test, presented in Figs. 12, 13 and 14, subjects the DET system to transient disturbances which cause it to go from an initial steady-state condition in the charge/shunt mode of operation to the boost mode and back to the charge/shunt mode in a period of 10 milliseconds. This transient response is caused by a step change in the system load current from 0 to 8 A at 1.7 milliseconds and back to zero at 6.7 milliseconds, while the solar array supplies 4 A of current continuously throughout the test. When no load current is being drawn, the entire 4 A of solar array current must be shunted from the bus to avoid an over-voltage condition. During this test, the signals corresponding to the battery

TABLE 1. Waveforms and Scales

WAVEFORM	VARIABLE	SCALE	RANGE
1	LOAD CURRENT	10 A/DIVISION	-50 TO + 10 A
2	SHUNT CURRENT	5 A/DIVISION	-20 TO + 10 A
3	BATTERY CURRENT	10 A/DIVISION	-30 TO + 30 A
4	BUS VOLTAGE	.5 V/DIVISION	27.5 TO 30.5 V

state of charge have been set to indicate a discharged condition, and therefore the battery is charged at a maximum rate of approximately 1.2 A. The remaining 2.8 A of solar array current is shunted into the shunt resistors. When the system loads require 8 A of current, however, the boost converter must be activated to supply the additional 4 A of load current required. The complete transition from charge/shunt to boost and back to charge/shunt operation is illustrated in Fig. 12. The horizonal scale for this figure is 1 millisecond per major division. The oscillograms are multiple exposures, and therefore the switching of the load current for each of the four traces does not necessarily occur at precisely the same position on the grid. Also, there is sometimes a zero offset in the measured results due to a drift in the oscilloscope between the multiple exposures.

The first 1.7 milliseconds of Fig. 12 illustrate steady-state operation in the charge/shunt mode. The bus voltage is steady at a level of approximately 28.2 volts. At 1.7 milliseconds, the required load current is switched from 0 to 8 A. This sudden change in load current causes a downward jump in the bus voltage due to the voltage drop across the equivalent series resistance of the output capacitor, r_{C2} of Fig. 8, of the boost converter. This capacitor had been charged to the steady-state value of bus voltage, 28.2 V, and at the instant of switching is the only source of current to supply the new load requirement. With this rapid drop in bus voltage to a new level corresponding to the boost mode of operation, the shunt elements and the battery charger turn off consecutively, and the boost converter turns on. This transient response is illustrated with an expanded time scale in Fig. 13, where the horizontal scale has been changed to 100 microseconds per major division, and the switching occurs at the .70 microseconds position of the trace. In this expanded view, it becomes clear that there is a delay of approximately 40 microseconds between the time the signal to turn off the shunt elements is generated and the time that the shunt current actually falls to zero. This delay, due primarily to the time required for operational amplifiers in the shunt drive circuitry to come out of saturation, causes the bus voltage to continue to fall even as the boost converter supplies additional current to the loads.

Looking again at Fig. 12, one sees that the shunt current does fall to zero and remains zero while the battery current decreases to a steady-state value of approximately -6 A, and the bus voltage settles to an average value

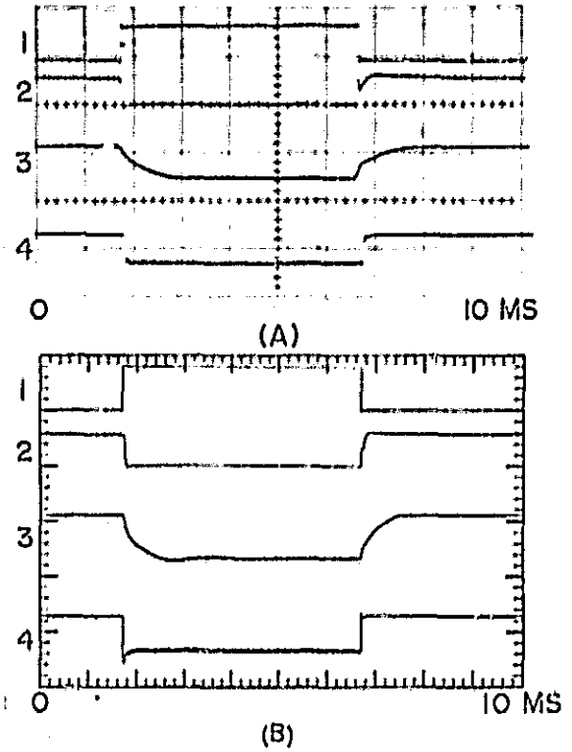

Fig. 12. Test Case I. Solar array current = 4A. Load current switches from 0 to 8 to 0 amperes.

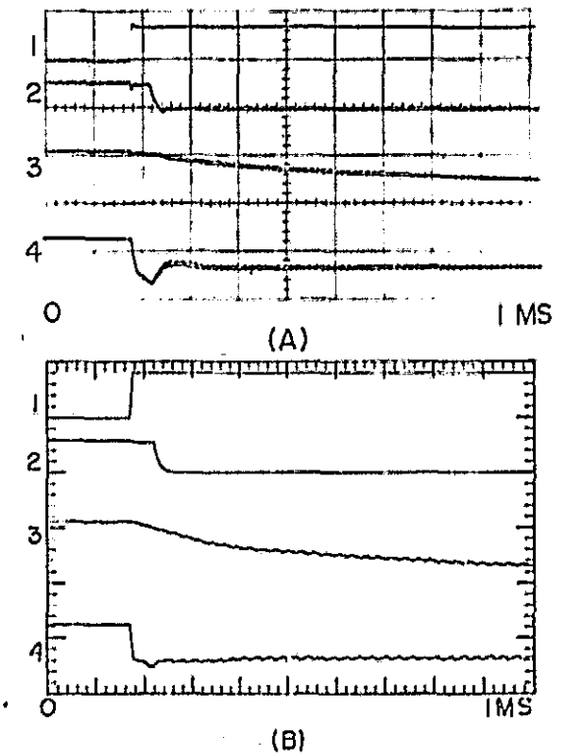

Fig. 13. Test Case I. Expanded view of 0 to 8 ampere switching transient.

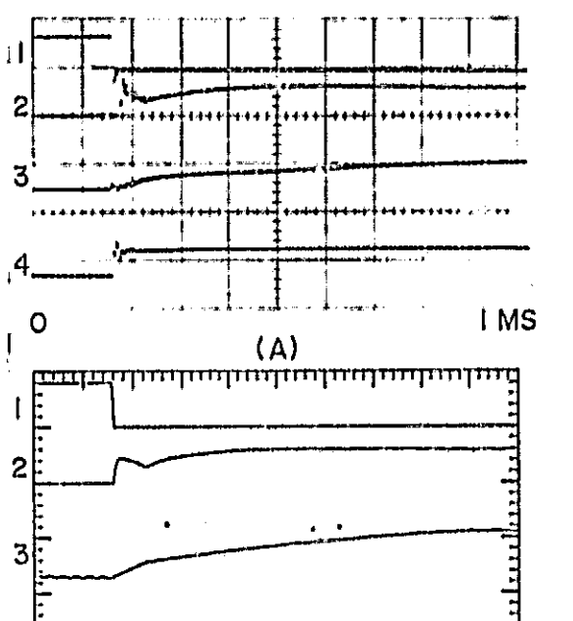

Fig. 14. Test Case I. Expanded view of 8 to 0 ampere switching transient.

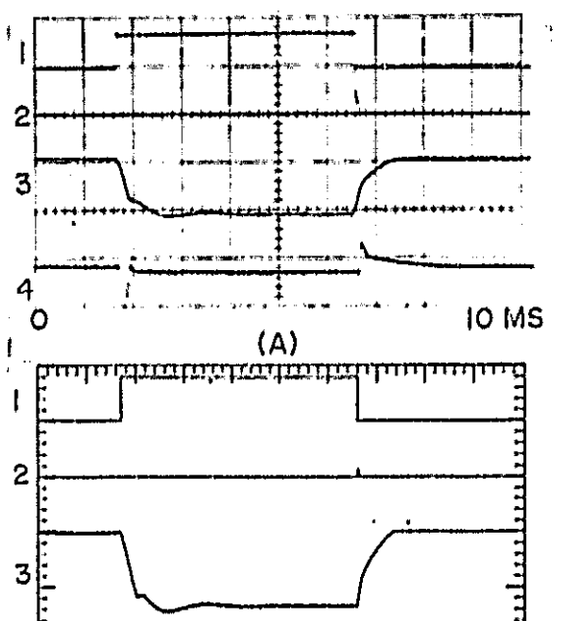

Fig. 15. Test Case II. Solar array current = 0A. Load current switches from 0 to 8 to 0 amperes.

of approximately 27.8 V. At approximately 6.7 milliseconds, the load current is switched back to zero, again causing a jump in the bus voltage, this time in the upward direction, due to the equivalent series resistance of the boost converter output capacitor. This switching transient is expanded in Fig. 14 where again the expanded time scale is 100 microseconds per major division. The bus voltage is seen to jump to a new level of approximately 28.2 V which demands that the boost converter turn off and that the energy stored in the output inductor of the boost converter, L_b in Fig. 8, as well as the 4 A solar array current be shunted from the bus.

As can be seen in Fig. 12, during the interval that the system is returning to a steady-state condition in the charge/shunt mode, the battery current does not change from -6 A to 1.2 A in a simple single-time-constant manner. The shape of this transient waveform is a very complex nonlinear function of the state variables of the system. As diodes and transistors are switched on and off and as energy stored in inductors and capacitors is depleted or increased, currents and voltages throughout the system undergo abrupt transitions and proceed along complex trajectories. It is beyond the intended scope of this paper to analyze this dynamic behavior in detail, but it should be pointed out that the computer-simulation waveforms presented in this section duplicate with considerable accuracy the shapes of the actual system responses and consequently the complex system interactions which cause them. It is therefore possible to use the computer simulation to examine any of the state variables which are used in describing the system, including the transformer flux, to determine more precisely the way in which the various subsystems interact to produce these observed waveforms. With the computer simulation, it is a simple matter to look at any or all of the system state variable trajectories, whereas when working with a breadboard unit it often is difficult, and sometimes impossible, to make accurate measments of the variables of interest.

A second test case is presented in Figs. 15, 16 and 17. Again, the same four waveforms are displayed in each figure with the vertical scales listed in Table 1. Throughout this test, the solar array is generating no current. The transient disturbance is again introduced by a step change in load from zero to 8 A and back to zero over a period of 10 milliseconds. Fig. 15 displays the entire 10 millisecond response. For the first 1.7 and the final 3.3 milliseconds of this display, no external load current is supplied. However, at all times the various control subsystems of this DET system require some power to operate continuously in a standby mode so as to be able to respond immediately to any system disturbance. When no solar array current is available, this standby power must be supplied by the battery through the boost converter, thus requiring the system to operate in the boost mode. The amount of current required to maintain this standby condition is approximately 100 mA and thus is not discernible in the graphic displays presented. The boost mode of operation is in evidence, however, when examining the bus voltage

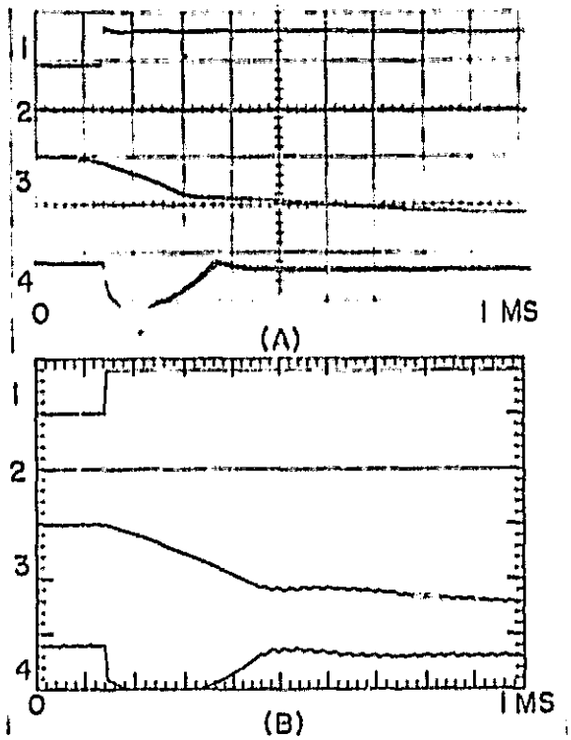

Fig. 16. Test Case II. Expanded view of 0 to 8 ampere switching transient.

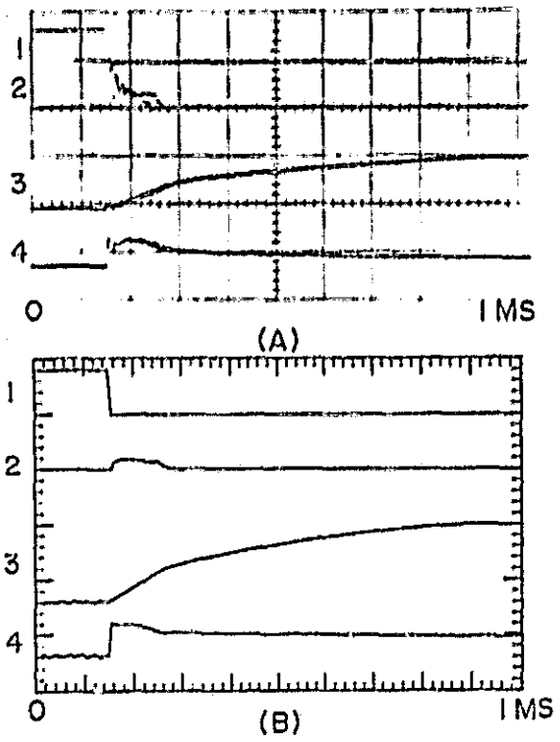

Fig. 17. Test Case II. Expanded view of 8 to 0 ampere switching transient.

waveform in Fig. 15. Over the last three milliseconds of this trace, the bus voltage slowly decays until the boost mode of operation is activated and the standby power is supplied through the boost converter.

At 1.7 milliseconds, the load current is switched from zero to 8 A and the system moves further into the boost mode of operation. This switching interval is illustrated with an expanded time scale of 100 microseconds per major division in Fig. 16. At 6.6 milliseconds the load current is switched back to zero and the transient of Fig. 17 results. When the 8 A load is removed from the bus, the bus voltage jumps upward to a value greater than 28 V as a result of the boost converter current suddenly flowing through the equivalent series resistance of the output capacitor, and the charge/shunt mode of operation is momentarily activated. The bus voltage quickly falls back inside the deadband region, however, and then slowly decays to the upper limit of the boost mode of operation in order to again supply the system standby power.

The presentation of experimental and corresponding simulation data in this section has, because of space limitations, been restricted to two test cases. These particular cases were selected from a large pool of data which was collected throughout this endeavor because the switched load tests cause the DET system, and likewise its computer simulation model, to function in each of the possible modes of operation, thus giving a fairly complete representation of its performance. The oscillograms and corresponding computer generated waveforms have been presented in a form which hopefully enables the reader to make a careful comparison and draw his own conclusions as to the accuracy of the simulation technique described in this paper. The simulation runs illustrated in Figs. 12(B) and 15(B) require approximately [illegible] hour of computation time, while each of the [illegible] millisecond runs requires approximately [illegible] minutes to complete the data display. As mentioned previously, the small computer used in this work was a PDP-11/45 with 16K words of memory using a disk operating system. The approximate cost per hour of computation, including purchase price amortization and maintainance, was ten dollars.

CONCLUSIONS

A digital computer simulation technique has been presented as a viable tool for the study of aggregate power-conditioning systems. As discussed earlier in the paper, a preliminary step in the development of such a system simulation is the postulation of a conceptual model. This model and its subsequent mathematical representation are of utmost importance in the simulation process, for it is at this level that the nature of the real system being simulated is captured. The computer program performs the repetitive computations necessary to generate system state trajectories, but the computations performed are dictated by the differential and functional equations developed to represent real system performance. The resultant computer simulations of actual

system trajectories can only be as accurate as the system model allows, and only those aspects of the system behavior which are included in the simulation model can be expected to appear in the computed results.

The examples presented above are not intended to be exhaustive. This paper presents the results of the development of a tool for use in studying power-processing systems which are too complex to be handled with classical analysis tools such as phase plane and linearization techniques. Having verified the validity and accuracy of this technique, it is intended that the computer model developed be fully exercised to aid in the final development of the DET system described above and to contribute, from the beginning stages, to the development of future power-conditioning systems. One of the proposed uses for this program is a parameter optimization study through repeated simulation runs to determine which values of selected components might improve some aspect of the system performance. This parameter modification can be accomplished quite easily within the simulation program, whereas considerable difficulty can sometimes be encountered when attempting such a study at the breadboard level. Other uses of such a program include the study of semiconductor component stresses within the system, especially during severe switching transients such as illustrated above ; and the study of system stability when in any of the modes of operation possible.

The digital computer technique described in this paper has been applied quite successfully to a particular direct-energy-transfer power-conditioning system of considerable complexity which is still in the development stages. The computer simulation of this system has been exercised vigorously and extensively in an attempt to verify its accuracy under all operating conditions and to demonstrate its usefulness. It is felt that the test data presented in this paper are a good representation of this testing. Moreover, it is believed that the functional block diagram approach used in this simulation technique possesses significant advantages over the network topology approach of other commonly available electronic circuit analysis programs when used to study such composite nonlinear dynamic systems.

REFERENCES

1. Space Power and Electric Propulsion, A Report for NASA prepared by the NASA Research and Technology Advisory Committee on Space Power and Electric Propulsion, Vol. 1, pp. 87-105, and Vol. 2, pp. 101-144, August 1972.

2. Y. Yu, J. J. Biess, A. D. Schoenfeld, and V. R. Lalli, "The Application of Standardized Control and Interface Circuits to Three DC to DC Power Converters," IEEE Power Electronics Specialists Conference Record, pp. 237-248, June 1973.

3. E. E. Landsman, "Modular Converters for Space Power Systems," IEEE Power Conditioning Specialists Conference Record, pp. 87-99, April 1970.

4. G. W. Wester and R. D. Middlebrook, "Low-Frequency Characterization of Switched DC-DC Converters," IEEE Trans. on Aerospace and Electronic Systems, Vol. AES-9, No. 3, pp. 376-385, May 1973.

5. F. C. Y. Lee, T. G. Wilson, and S. Y. M. Feng, "Analysis of Limit Cycles in a Two-Transistor Saturable Core Parallel Inverter," IEEE Trans. on Aerospace and Electronic Systems, Vol. AES-9, No. 4, pp. 571-584, July 1973.

6. T. T. Nishizaki, R. G. Aiken, and G. J. R. St. Amand, "Computer-Aided Design and Weight Estimation of High-Power High-Voltage Power Conditioners," IEEE Trans. on Aerospace and Electronic Systems, Vol. AES-7, No. 6, pp. 1179-1194, November 1971.

7. A. K. Ohri, H. A. Owen, Jr., T. G. Wilson, and G. E. Rodriguez, "Digital Computer Simulation of Inductor-Energy-Storage DC-to-DC Converters with Closed-Loop Regulators," S. P. 103, ESRO Spacecraft Power Conditioning Electronics Seminar, Frascati, Italy, May 1974.

8. A. Capel, J. G. Ferrante, and R. Prajoux, "Stability Analysis of a PWM Controlled DC/DC Regulator with DC and AC Feedback Loops," IEEE Power Electronics Specialists Conference Record, pp. 246-254, June 1974.

9. 1130 Continuous System Modeling Program: Program Description and Operations Manual, IBM manual GH20-0282-2.